

# Lithium Superoxide Encapsulated in a Benzoquinone Anion Matrix

Matthew Nava<sup>a,b</sup>, Shiyu Zhang<sup>a,c</sup>, Katharine S. Pastore<sup>d</sup>, Xiaowen Feng<sup>b</sup>, Kyle M. Lancaster<sup>d</sup>, Daniel G. Nocera<sup>b,1</sup>, and Christopher C. Cummins<sup>a,1</sup>

<sup>a</sup>Department of Chemistry, Massachusetts Institute of Technology, Cambridge MA, United States 02139-4307; <sup>b</sup>Department of Chemistry and Chemical Biology, Harvard University, 12 Oxford Street, Cambridge MA, United States; <sup>c</sup>Current Address: Department of Chemistry and Biochemistry, The Ohio State University, 151 West Woodruff Ave., Columbus OH, 43210, United States; <sup>d</sup>Department of Chemistry and Chemical Biology, Baker Laboratory, Cornell University, Ithaca, NY, 14853, United States

This manuscript was compiled on April 4, 2022

1 Lithium peroxide is the crucial storage material in lithium-air batteries. Understanding the redox properties of this salt is paramount towards improving the performance of this class of batteries. Lithium peroxide, upon exposure to *p*-benzoquinone ( $p\text{-C}_6\text{H}_4\text{O}_2$ ) vapor, develops a deep blue color. This blue powder can be formally described as  $[\text{Li}_2\text{O}_2]_{0.3}\cdot[\text{LiO}_2]_{0.7}\cdot\{\text{Li}[p\text{-C}_6\text{H}_4\text{O}_2]\}_{0.7}$ , though spectroscopic characterization indicates a more nuanced structural specification. Infrared, Raman, electron paramagnetic resonance, diffuse-reflectance UV-vis and X-ray absorption spectroscopy reveal that the lithium salt of the benzoquinone radical anion forms on the surface of the lithium peroxide, indicating the occurrence of electron and lithium ion transfer in the solid state. As a result, obligate lithium superoxide is formed and encapsulated in a shell of  $\text{Li}[p\text{-C}_6\text{H}_4\text{O}_2]$  with a core of  $\text{Li}_2\text{O}_2$ . Lithium superoxide has been proposed as a critical intermediate in the charge/discharge cycle of Li-air batteries but has yet to be isolated owing to instability. The results reported herein provide a snapshot of lithium peroxide/superoxide chemistry in the solid state with redox mediation.

Lithium superoxide | Lithium peroxide oxidation | Li-air battery

1 The advent of metal-air batteries has provided impetus for understanding the structure, spectroscopic properties and chemical reactivity of various metal oxides. Lithium-air batteries, which possess a theoretical energy density approaching that of liquid fuels, have emerged as potential candidates to replace lithium-ion batteries (1–4). Lithium-air batteries operate by electron transfer from a high surface area cathode to oxygen gas during discharge, generating lithium peroxide deposits. Upon charging, the lithium peroxide is oxidized back to oxygen gas. Despite demonstrating promise as a replacement for lithium-ion batteries, this electrochemical energy storage system suffers from numerous challenges that must be overcome (5–8), the most important of which is reversible charging.

15 Lithium superoxide,  $\text{LiO}_2$ , is an important intermediate in both the reduction of oxygen to lithium peroxide and oxidation of lithium peroxide back to oxygen (9–13). Lithium superoxide, *via* disproportionation, is thought to be responsible for the growth of large lithium peroxide toroids commonly observed during discharge of nonaqueous lithium-air cells, but is also implicated in numerous studies (14–18) as being responsible, either directly or through the intermediacy of  $^1\text{O}_2$  (19, 20), for the degradation of the organic solvent and electrolyte in the battery. Furthermore, ‘superoxide like’ sites on the surface of lithium peroxide are thought to be responsible for both enhanced reactivity with electrolytes in lithium-air batteries and enhanced conductivity (21, 22).

28 While the superoxide salts of cesium, rubidium, potassium



Fig. 1. The vapor diffusion setup used to prepare  $[\text{Li}_2\text{O}_2]_{0.3}\cdot[\text{LiO}_2]_{0.7}\cdot\{\text{Li}[p\text{-C}_6\text{H}_4\text{O}_2]\}_{0.7}$ . The setup consists of a small vial that contains  $\text{Li}_2\text{O}_2$  sealed within a larger vial containing  $p\text{-C}_6\text{H}_4\text{O}_2$ . The vial on the left is a freshly prepared sample, while the vial on the right has been allowed to stand at room temperature for a month.

and sodium are well known, and potassium superoxide is commercially available, the lithium salt of superoxide was not observed definitively until recently in noble gas matrices at low temperatures (23–27). Matrix isolation studies have

## Significance Statement

Lithium superoxide ( $\text{LiO}_2$ ) is an important intermediate in lithium-air batteries, a promising next-generation energy storage platform. The conductivity, stability and reactivity profiles of  $\text{LiO}_2$  are thought to play a crucial role in the cyclability of lithium-air batteries. We demonstrate that physical encapsulation of  $\text{Li}_2\text{O}_2$  with an appropriate redox-active molecule may be a viable strategy to access and stabilize  $\text{LiO}_2$  at room temperature while simultaneously protecting the solvent and electrolyte from deleterious reactivity derived from  $\text{LiO}_2$ . Encapsulation with a redox mediator does not impede interfacial electron and lithium-ion transport and provides researchers with a model system that recapitulates the charging of a lithium-air cell.

M.N., S.Z., C.C.C. and D.G.N. designed research; M.N. and S.Z. performed research; M.N., S.Z., K.E.P., X.F. and K.M.L. contributed analytical tools; M.N., S.Z., K.E.P., K.M.L., C.C.C. and D.G.N. analyzed data; and M.N., C.C.C., and D.G.N. wrote the paper.

The authors declare no competing interest.

<sup>1</sup>To whom correspondence should be addressed. E-mail: ccummins@mit.edu; dnocera@fas.harvard.edu

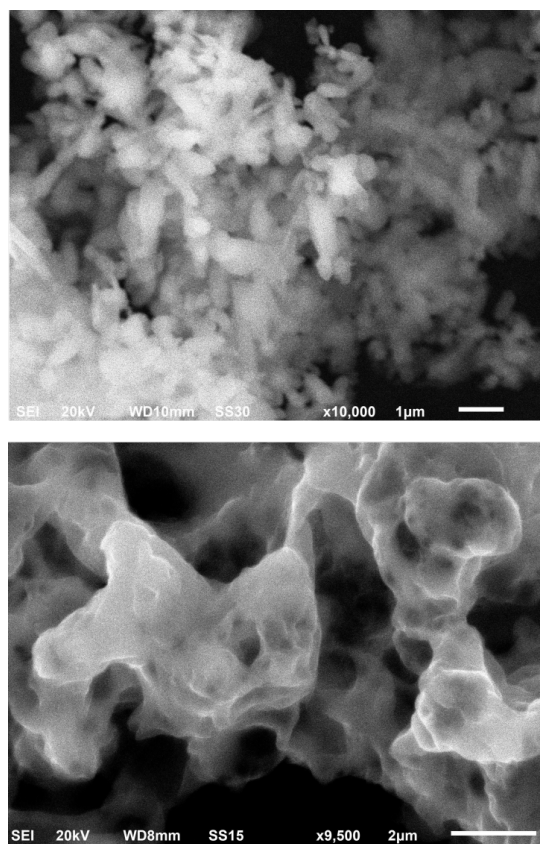


Fig. 2. SEM images of commercial  $\text{Li}_2\text{O}_2$  (top) and **1** (bottom). Fusing of the  $\text{Li}_2\text{O}_2$  particles is evident in **1**.

demonstrated that the infrared absorption peak associated with the O–O stretch of superoxide loses approximately 80% of its intensity when warmed from 15 to 34 K. Two additional reports of the cryogenic preparation of  $\text{LiO}_2$  exist: one with  $\text{O}_3$  and  $\text{Li}_2\text{O}_2$  in freon at  $-65^\circ\text{C}$  (28), and another involving treatment of  $\text{O}_2$  with lithium metal in  $\text{NH}_3$  at  $-78^\circ\text{C}$  (29).

Strides have also been made towards observing or directly stabilizing lithium superoxide in lithium-air batteries (30–32). At room temperature lithium superoxide, if unstabilized, is expected to have a fleeting existence, prompting a study to experimentally demonstrate that Raman signals assigned to lithium superoxide in earlier lithium-air works may be ascribed to polyvinylidene fluoride (PVDF) binder which has undergone a dehydrohalogenation reaction (33). However, a subsequent report has asserted that rigorous drying of the PVDF binder precludes the dehydrohalogenation reaction (34). Indeed, the presence and involvement of observable lithium superoxide in lithium-air batteries remains a topic of interest and some controversy (35).

The continued advancement of lithium-air batteries will require improved characterization and understanding of the properties of lithium superoxide, particularly with respect to elucidating the fundamental properties of the salt in the solid state. Reported herein is a solid-state material that models the oxidation of lithium peroxide to lithium superoxide, with a surface coating of *p*-benzoquinone acting as the electron acceptor. The system recapitulates the proposal of ‘superoxide like’ sites on the surface of lithium peroxide in lithium-air batteries.

## Results

**Synthesis.** Lithium peroxide was oxidized by *p*-benzoquinone ( $p\text{-C}_6\text{H}_4\text{O}_2$ ) using a setup similar to that of growing crystals with two organic solvents (Fig. 1). Vapor diffusion of  $p\text{-C}_6\text{H}_4\text{O}_2$  (vapor pressure = 0.1 mm Hg at  $25^\circ\text{C}$ ) (36) onto solid lithium peroxide resulted in a gradual color change initially to very faint blue, followed by considerable darkening over the course of several weeks to furnish a sample that ultimately appeared black. This material, designated as compound **1**, was thermodynamically unstable and detonated upon scratching with a metal spatula presumably releasing oxygen (**caution!**); for this reason use of a plastic spatula was preferred.

To accelerate the diffusion of  $p\text{-C}_6\text{H}_4\text{O}_2$  onto  $\text{Li}_2\text{O}_2$ , these reactants were placed together as solids into a sealed ampule and heated at  $70^\circ\text{C}$  under a slight vacuum overnight to produce the identical black color as observed for the material prepared via the vapor diffusion method. Comparison of the spectroscopic data for **1** (*vide infra*) produced by these two different methods established the materials to be identical. Sampling by gas chromatography the headspace gases generated, if any, when using the accelerated ampule synthesis method showed that oxygen gas was not evolved.

Phenylboronic acid is easily oxidized to phenol by hydrogen peroxide generated *in situ* by hydrolysis of either peroxide or superoxide salts (37). Aqueous titration of **1** with phenylboronic acid gave nearly quantitative conversion to phenol, as verified by nuclear magnetic resonance (NMR) spectroscopy (*SI Appendix*, Fig. S1). This result confirms that the O–O bonds remains intact in **1** and reinforces the conclusion that a negligible amount of  $\text{O}_2$  gas is released during the formation of **1**.

Curiously, using an equimolar ratio of  $\text{Li}_2\text{O}_2$  and  $p\text{-C}_6\text{H}_4\text{O}_2$  in a sealed ampule to produce **1** consistently resulted in small amounts of  $p\text{-C}_6\text{H}_4\text{O}_2$  that were observed to sublime to the top of the ampule, indicating that the molar ratio of  $\text{Li}_2\text{O}_2$  and  $p\text{-C}_6\text{H}_4\text{O}_2$  is not 1:1 in compound **1**. The chemical formula of **1** as determined by C and H elemental analysis indicates limiting detailed formulations of either  $[\text{Li}_2\text{O}_2]_{0.3}[\text{LiO}_2]_{0.7}\{\text{Li}[p\text{-C}_6\text{H}_4\text{O}_2]\}_{0.7}$  or  $[\text{Li}_2\text{O}_2]\cdot[p\text{-C}_6\text{H}_4\text{O}_2]_{0.7}$ . Furthermore, unconsumed  $p\text{-C}_6\text{H}_4\text{O}_2$  can be recovered from the 1:1 reaction in quantities consistent with our established chemical formula of **1**. Running the synthesis of **1** using an excess of  $p\text{-C}_6\text{H}_4\text{O}_2$  also does not result in fractional compositions of  $p\text{-C}_6\text{H}_4\text{O}_2$  exceeding 0.7, as the excess  $p\text{-C}_6\text{H}_4\text{O}_2$  is recovered following its sublimation from the black solid sample of **1**.

Examination of **1** by scanning electron microscopy (SEM, Fig. 2) revealed distinct morphological changes as compared with the  $\text{Li}_2\text{O}_2$  starting material. Commercial  $\text{Li}_2\text{O}_2$ , as purchased, is composed of particles several hundred nanometers in diameter. Upon exposure of  $\text{Li}_2\text{O}_2$  to  $p\text{-C}_6\text{H}_4\text{O}_2$ , fusing of particles was observed, suggesting that the black material that formed on the outer surface of the peroxide causes the particles to coalesce (Fig. 2 and *SI Appendix*, Fig. S2).

The blue color of quinone monoanions (38, 39) prompted us to independently prepare  $\text{Li}[p\text{-C}_6\text{H}_4\text{O}_2]$  (**2**), to determine whether the benzoquinone anion radical is responsible for the black color of **1**. As the lithium salt of the dianion,  $\text{Li}_2[p\text{-C}_6\text{H}_4\text{O}_2]$ , is known, a comproportionation strategy was pursued. Using the vapor-diffusion method, it was found that **2** could be prepared from  $\text{Li}_2[p\text{-C}_6\text{H}_4\text{O}_2]$  and  $p\text{-C}_6\text{H}_4\text{O}_2$  as an intense blue powder. Salt **2** could also be prepared via mechan-

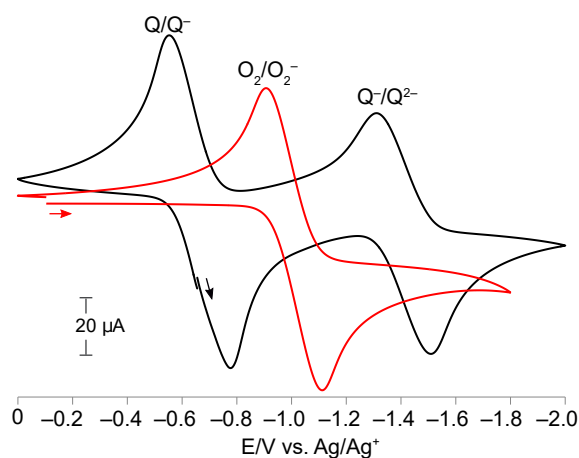


**Fig. 3.** Cyclic voltammograms of  $p\text{-C}_6\text{H}_4\text{O}_2$  (Q) at 4.8 mM (black trace) and saturated  $\text{O}_2$  (red trace) in DMF with [TBA]  $\text{PF}_6$  supporting electrolyte. The working electrode was a glassy carbon button electrode, paired with a platinum counter electrode and a  $\text{Ag}/\text{Ag}^+$  reference electrode. Scan rate = 20 mV/s. The superoxide/peroxide couple is omitted due to its irreversible nature.

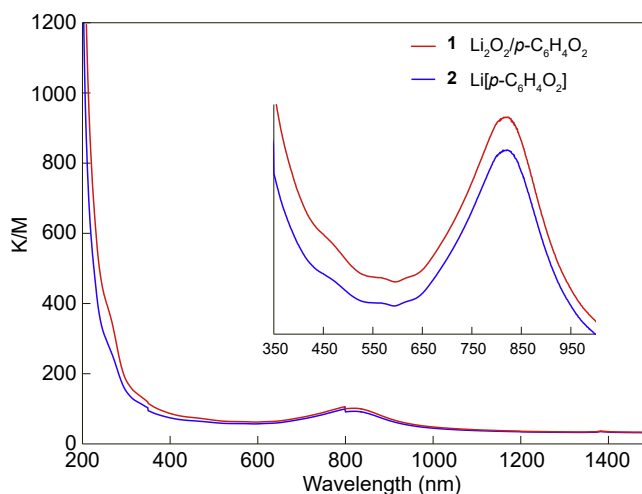


**Fig. 4.** Diffuse reflectance UV-vis spectra of **1** (red) and **2** (blue). The inset is corrected for a light source change of the UV-vis spectrophotometer at 800 nm.

123 ical mixing of  $\text{Li}_2[p\text{-C}_6\text{H}_4\text{O}_2]$  and  $p\text{-C}_6\text{H}_4\text{O}_2$  in a mortar and  
 124 pestle. Vapor diffusion or mechanical mixing gave samples of  
 125 **2** having indistinguishable properties, with the latter method  
 126 better suited for producing larger quantities of the salt. When  
 127 samples of **2** are heated above  $70^\circ\text{C}$  and under vacuum, the  
 128 disproportionation reaction prevails to furnish  $\text{Li}_2[p\text{-C}_6\text{H}_4\text{O}_2]$   
 129 (*SI Appendix*, Figs. S3 and S4). Hence, the successful synthesis  
 130 of **1** from  $\text{Li}_2\text{O}_2$  and  $p\text{-C}_6\text{H}_4\text{O}_2$  (*vide supra*) was achieved for  
 131 temperatures at or below  $70^\circ\text{C}$ .

132 Fig. 3 displays overlaid, separately-acquired cyclic voltam-  
 133 mograms for the reduction of  $\text{O}_2$  and  $p\text{-C}_6\text{H}_4\text{O}_2$  in DMF with  
 134 tetrabutylammonium ([TBA]  $\text{PF}_6$ ) hexafluorophosphate electrolyte.  
 135 The irreversible electrochemistry of oxygen and quinone asso-  
 136 ciated with lithium cations was avoided with [TBA] $\text{PF}_6$   
 137 supporting electrolyte but such a substitution results in an  
 138 approximately several hundred millivolt cathodic shift relative  
 139 to their lithium potentials (40, 41).  $p\text{-C}_6\text{H}_4\text{O}_2$  has two re-  
 140 versible reductions corresponding to the  $0/-$  and  $-/2-$  couples  
 141 at  $-0.67\text{ V}$  and  $-1.42\text{ V}$  vs  $\text{Ag}/\text{Ag}^+$ . The reduction of oxygen  
 142 to superoxide falls between the two reduction potentials of the  
 143 quinone at  $-1.02\text{ V}$  vs  $\text{Ag}/\text{Ag}^+$ .

144 **Spectroscopy.** Fig. 4 displays the diffuse reflectance UV-vis  
 145 spectrum (DRUVS) of **1**. The visible spectral region is do-  
 146 minated by a pronounced absorption band with  $\lambda_{max} = 825\text{ nm}$ ,  
 147 accounting for the blue color of the compound. Salt **2**, pre-  
 148 pared by mechanical grinding, exhibits an identical absorption  
 149 band. The only notable difference between the absorption  
 150 profiles of **1** and **2** is that the former spectrum exhibits a  
 151 more pronounced shoulder at  $\lambda = 250\text{ nm}$ ; superoxide exhibits  
 152 an absorption at this wavelength (42).

153 EPR spectra of **1** and **2** (Fig. 5) display a single broad  
 154 signal centered at  $g = 2.008$ , a feature consistent with the  
 155 presence of a spin one-half organic radical. Hyperfine coupling  
 156 could not be resolved at 77 K or by dilution of the samples  
 157 with sodium sulfate due to the close intermolecular contact of  
 158 the spin bearing species composing both samples (*vide infra*).  
 159 EPR spin quantification, a method used to determine the  
 160 number of radicals present in a bulk sample, was performed by

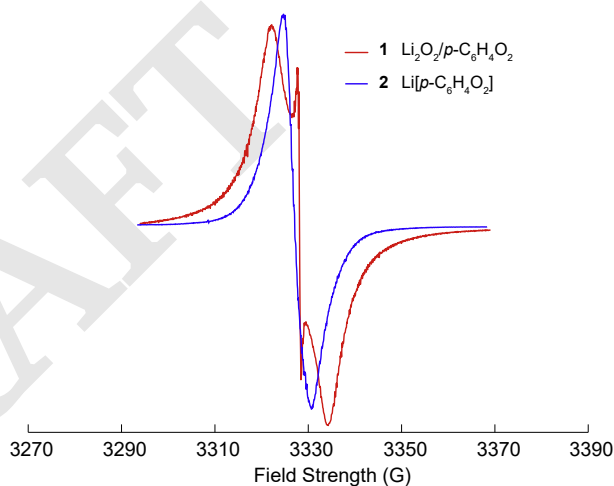


**Fig. 5.** EPR spectra of **1** and **2** collected at 77 K.

161 spin integration of **2** against an EPR quantification standard  
 162 2,2-diphenyl-1-picrylhydrazyl (DPPH) and indicated the spin  
 163 yield (the ratio of the number of observed spins against the  
 164 expected number of spins) of **2** to be 2.4% (*SI Appendix*,  
 165 Fig. S5). A broad EPR signal derived from a powdered  
 166 sample of the alkali quinone radical anion  $\text{Na}[o\text{-C}_6\text{Cl}_4\text{O}_2]$  has  
 167 been observed previously (43) and similar spin yields (0.1 to  
 168 10%) have been measured for quinone radical anions (44). A  
 169 noteworthy feature of the EPR spectrum of **1**, although not  
 170 always as pronounced, is the presence of an additional narrow  
 171 line at  $g = 2.009$ . Powdered potassium superoxide exhibits a  
 172 similarly narrow line in its EPR spectrum (45). The presence  
 173 of superoxide in **1** as suggested by the EPR data is further  
 174 supported by SQUID magnetometry. Subtraction of the DC  
 175 susceptibility of **2** from that of **1** (mass corrected, *SI Appendix*,  
 176 Fig. S6) indicates an additional paramagnetic species in **1**,  
 177 consistent with the presence of superoxide.

178 Infrared (IR) spectroscopy was used to determine the redox  
 179 level of the benzoquinone present in **1**. The position of the  
 180  $\text{C}=\text{C}$  and  $\text{C}-\text{O}$  infrared stretches of quinones are sensitive  
 181 to the reduction state of the molecule, with red-shifting of

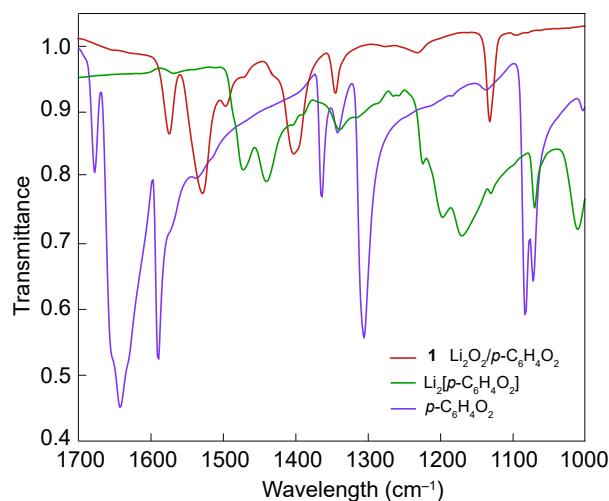


**Fig. 6.** ATR-IR spectra of **1** (red),  $p\text{-C}_6\text{H}_4\text{O}_2$  (purple) and  $\text{Li}_2[p\text{-C}_6\text{H}_4\text{O}_2]$  (green) from 1000 to  $1700\text{ cm}^{-1}$ .

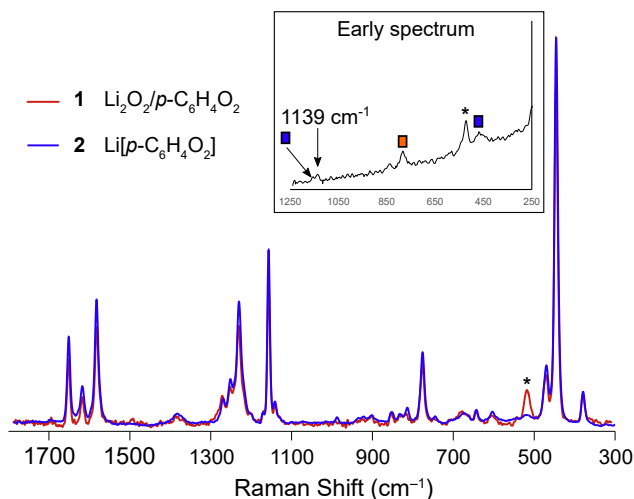


**Fig. 7.** Raman spectral overlay of **1** (red) and **2** (blue). The inset shows a Raman spectrum acquired during the early stages of  $p$ -benzoquinone vapor absorption on  $\text{Li}_2\text{O}_2$ ; a band in the region typically associated with superoxides is observable prior to the formation of an optically thick coating of  $\text{Li}[p\text{-C}_6\text{H}_4\text{O}_2]$  on **1**. Asterisks indicate bands associated with quartz capillaries while boxes above peaks indicate bands associated with  $\text{Li}_2\text{O}_2$  (orange) or  $p$ -benzoquinone $^{0/-1}$  (blue).

the aforementioned vibrations occurring upon reduction of quinone to the quinone radical anion and finally to the dianionic phenolate salt. The IR spectrum of **1** is superimposed with that of  $p\text{-C}_6\text{H}_4\text{O}_2$  and  $\text{Li}_2[p\text{-C}_6\text{H}_4\text{O}_2]$  in Fig. 6.  $p$ -Benzoquinone has asymmetric and symmetric C=O stretches at  $1670$  and  $1646\text{ cm}^{-1}$ , respectively (46). The C=C stretch of  $p$ -benzoquinone is coupled to the two C=O stretches and is observed at  $1578\text{ cm}^{-1}$ . The C=C stretches of  $\text{Li}_2[p\text{-C}_6\text{H}_4\text{O}_2]$  are observed from  $1475\text{--}1442\text{ cm}^{-1}$  and the C—O stretch is likely centered at  $1172\text{ cm}^{-1}$ , clearly contrasting with that of  $p$ -benzoquinone. The C=O and C=C stretches of **1** fall between those of both  $p\text{-C}_6\text{H}_4\text{O}_2$  and  $\text{Li}_2[p\text{-C}_6\text{H}_4\text{O}_2]$ , with tentative assignments of the C=C stretches at  $1531\text{ cm}^{-1}$  and the C=O stretch at  $1405\text{ cm}^{-1}$ . These values compare favorably with data for spectroelectrochemically generated  $p$ -benzoquinone radical anion, which has assigned values of  $1506\text{ cm}^{-1}$  and  $1347\text{ cm}^{-1}$  for the C=C and C=O stretches, respectively (47). Broad bands associated with the Li—O stretches of  $\text{Li}_2\text{O}_2$  are observed in the infrared spectrum of **1** below  $600\text{ cm}^{-1}$  (SI Appendix, Fig. S7A).

The resonance Raman spectrum of **1** is overlaid with that of **2** in Fig. 7. The spectra of **1** and **2** are nearly identical, and are consonant with that reported for  $p$ -benzoquinone radical anion in solution (47). Comparison of the Raman spectrum of **2** with that of  $p\text{-C}_6\text{H}_4\text{O}_2$  and  $\text{Li}_2[p\text{-C}_6\text{H}_4\text{O}_2]$  support the notion that the redox level of **2** is that of a monoanion (SI Appendix, Figs. S8 and S9). Noticeably absent from the Raman spectrum of **1** are lines due to  $\text{Li}_2\text{O}_2$ . The strong absorption band of  $\text{Li}[p\text{-C}_6\text{H}_4\text{O}_2]$  at  $825\text{ nm}$  results in attenuation of the  $785\text{ nm}$  Raman excitation light below the surface of the particles of **1**. Accordingly, only the surface of **1** is resonance enhanced and as a consequence,  $\text{Li}_2\text{O}_2$  and  $\text{LiO}_2$  if present, are not observed. In an effort to break apart the light-attenuating surface coating, samples of **1** were gently compressed between microscope slides; however, the Raman spectrum of these crushed samples were identical to that shown in Figure 7. The inability to readily observe  $\text{LiO}_2$  in samples of **1** prompted studies focused on the *in situ* monitoring of the conversion of  $\text{Li}_2\text{O}_2$  to **1** (SI Appendix, S3.4). Upon the layering of  $p$ -benzoquinone on powdered  $\text{Li}_2\text{O}_2$  in a quartz capillary, a

blue gradient developed across the  $\text{Li}_2\text{O}_2$  (SI Appendix, Fig. S10). Raman spectral analysis along this gradient revealed the presence of a weak band at  $1139\text{ cm}^{-1}$  (inset, Fig. 7) superimposed on a highly fluorescent background. This band was not attributable to  $p$ -benzoquinone or its radical anion (SI Appendix, Fig. S11), is in a region typically associated with superoxide O—O stretches (32), and may be that of  $\text{LiO}_2$  present in the sample.

Oxygen K-edge ( $1s \rightarrow$  valence) X-ray absorption spectroscopy (XAS) was used to differentiate the natures of oxygen present in **1**. Oxygen K-edge XAS of **1**, **2**,  $\text{Li}_2\text{O}_2$  and  $\text{Li}_2[p\text{-C}_6\text{H}_4\text{O}_2]$  were collected and the corresponding data are presented in Fig. 8; the fitted peak energies are shown in SI Appendix, Fig. S12 and summarized in SI Appendix, Table S4. In general, the oxygen K-edge  $\pi^*$  features of C=O are at lower energy than the  $\sigma^*$  features of O—H (48). A detailed report of the electron energy loss spectra (EELS) of  $p$ -benzoquinone, hydroquinone, and phenol gives assignments of these features based on molecular orbital theory (49).

The  $\pi^*$  feature of  $p\text{-C}_6\text{H}_4\text{O}_2$  is at  $529.85\text{ eV}$ , and the  $\sigma^*$  feature of OH in hydroquinone is at  $534.6\text{ eV}$ . The presence of Li in the bonding environment of  $\text{Li}_2\text{O}_2$  shifts the  $\sigma^*$  O—O feature to  $531.6\text{ eV}$ , which is lower energy as compared to that of  $\text{H}_2\text{O}_2$ . Two peaks of about equal intensity in the spectrum of  $\text{Li}_2[p\text{-C}_6\text{H}_4\text{O}_2]$  at  $529.9\text{ eV}$  and  $532.6\text{ eV}$  are also in the spectrum of the independently prepared samples of **2** reported here, although the higher energy peak is of much higher relative intensity. If we attribute the first peak to the  $\pi^*$  C=O and the second to  $\sigma^*$  O—Li, since it is shifted by  $2\text{ eV}$  from literature  $\sigma^*$  O—H, the data are consistent with formation of the quinone radical in **2**, with some unreacted or reoxidized quinone present. The broad peak in **1** attributed to  $\text{Li}_2\text{O}_2$  obscures energetically proximate features, if any, however, the fitted peak at  $532.3\text{ eV}$  may come from  $\text{Li}[p\text{-C}_6\text{H}_4\text{O}_2]$  as supported by the comparison with the genuine spectrum of **2**.

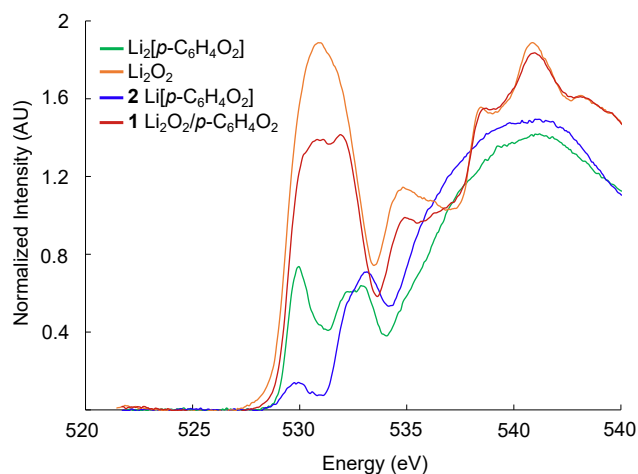


**Fig. 8.** Overlaid O K-edge XAS spectra of compounds  $\text{Li}_2[p\text{-C}_6\text{H}_4\text{O}_2]$ , **2**,  $\text{Li}_2\text{O}_2$ , and **1**.

color change of  $p\text{-C}_6\text{H}_4\text{O}_2$  from yellow to blue (and ultimately, black), which is indicative of reduction of  $p\text{-C}_6\text{H}_4\text{O}_2$ . Similarly, reactions **4** and **5** may be dismissed as analysis of the reaction headspace by GC did not reveal any oxygen production. Moreover, results from the titration of the product with  $\text{PhB}(\text{OH})_2$  to produce  $\text{PhOH}$  quantitatively suggest that no  $\text{O}_2$  was lost from the sample; the oxygen speciation has an O–O bond of peroxide or superoxide, and peroxide can directly oxidize boronic acids while superoxide may convert to peroxide upon disproportionation in water (37, 51–53). Additionally, the cyclic voltammograms in Fig. 3 show that it is thermodynamically unfavorable for the radical anion of  $p\text{-C}_6\text{H}_4\text{O}_2$  to oxidize superoxide to produce  $\text{O}_2$ . Reactions **2** and **3** depict electron transfer and lithium ion diffusion from lithium peroxide to benzoquinone, to generate lithium superoxide and either the benzoquinone radical monoanion or dianion, respectively. The spectroscopic properties of **2** rule out reaction **3** and point to reaction **2** as being operative.

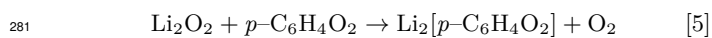
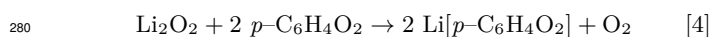
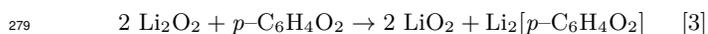
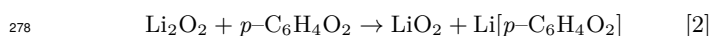
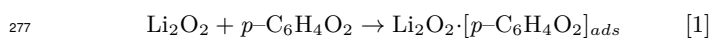
The radical monoanion of  $p\text{-C}_6\text{H}_4\text{O}_2$  has been studied in great detail and can be prepared by a variety of methods, such as pulse radiolysis of the neutral quinone in matrices (54) or frozen solutions (55), or direct reduction of  $p\text{-benzoquinone}$  with potassium in the presence of Kryptofix® 222 or crown ethers in THF (56). The  $\text{Li}^+$  salt of  $p\text{-C}_6\text{H}_4\text{O}_2$  radical monoanion is less studied, and only a handful of instances detailing the preparation of this compound are known (57–60). We therefore sought to prepare  $\text{Li}[p\text{-C}_6\text{H}_4\text{O}_2]$  (**2**) independently. We pursued the solid-state comproportionation reaction of  $\text{Li}_2[p\text{-C}_6\text{H}_4\text{O}_2]$ , prepared by known methods (50), with  $p\text{-C}_6\text{H}_4\text{O}_2$  to deliver **2**, as supported by a host of spectroscopic techniques: (i) the  $S=1/2$  EPR signal of Fig. 5; (ii) the energy of the C=O stretching frequency (in IR and Raman spectra, Figs. 6 and 7) of **2** is intermediate between  $p\text{-C}_6\text{H}_4\text{O}_2$  and the  $\text{Li}_2[p\text{-C}_6\text{H}_4\text{O}_2]$ , and; (iii) the XAS spectrum of **2** exhibits one major peak in the O 2p K-edge (as opposed to two peaks for the dianion). The viability of driving the comproportionation reaction to produce **2** using mechanical mixing was confirmed by Raman spectroscopy. Comparison of the Raman spectrum of **2** with those of  $\text{Li}_2[p\text{-C}_6\text{H}_4\text{O}_2]$  and  $p\text{-C}_6\text{H}_4\text{O}_2$  (SI Appendix, Figs. S8, S9) demonstrates the formation of  $\text{Li}[p\text{-C}_6\text{H}_4\text{O}_2]$  upon mixing.

The UV-vis absorption profile of **1** is strikingly similar to that of **2**. The dark blue color of the two materials is a result of identical absorption bands centered at 825 nm (Fig. 4). This absorbance is strikingly similar to semiquinone radical anions prepared in anhydrous *t*-butanol (57) and reminiscent of that arising from the  $\pi$  dimer exciplex formed upon the reduction of 2,3-dichloro-5,6-dicyano-1,4-benzoquinone (DDQ) (38, 39). In the cases of **1** and **2**,  $\pi$ -stacking between quinone radical anions may be facilitated by lithium counterions bridging the oxygens of neighboring quinone radical anions. The absorption band of weaker intensity at 460 nm in **1** and **2** has been ascribed to the  ${}^2B_{2g} \rightarrow {}^2B_{3u}$  HOMO-LUMO electronic transition of benzoquinone radical anion (47, 61). This transition exhibits a strong dependence on the solvent environment, with values of the absorption maximum ranging from 427 nm in water to 454 nm in pyridine. The UV-vis spectrum of both powdered potassium superoxide (45) and superoxide in solution have been reported (42, 62, 63). Superoxide in solution has an absorption max at 250 nm while solid potassium superoxide's absorption max is 350 nm and tails out to 600 nm. Strong

**Powder X-ray Diffraction (PXRD).** The PXRD pattern of **1** is shown in Fig. 9. The pattern is a composite of contributions from **2** (blue bars) and  $\text{Li}_2\text{O}_2$  (orange bars). The peaks of **1** labeled with blue bars in Fig. 9 coincide with the PXRD pattern of an independently prepared sample of authentic **2** (SI Appendix, Fig. S13D). SI Appendix, Fig. S13C displays a comparison of the PXRD patterns of **2** to  $\text{Li}_2[p\text{-C}_6\text{H}_4\text{O}_2]$ ; none of the PXRD peaks of  $\text{Li}_2[p\text{-C}_6\text{H}_4\text{O}_2]$  (50) are observed in samples of **1**. The majority of the diffraction peaks in **1** coincide with those of **2** or  $\text{Li}_2\text{O}_2$ ; the presence of both these species in **1** is consistent with the formulation of  $[\text{Li}_2\text{O}_2]_{0.3} \cdot [\text{LiO}_2]_{0.7} \cdot \{\text{Li}[p\text{-C}_6\text{H}_4\text{O}_2]\}_{0.7}$ . The peaks labeled with asterisks in Figure 9 are of unknown origin, but could be posited tentatively to arise from  $\text{LiO}_2$ .

## Discussion

$p\text{-Benzoquinone}$ , a yellow solid at room temperature, has a high vapor pressure. The surface of lithium peroxide exposed to  $p\text{-C}_6\text{H}_4\text{O}_2$  develops an intense blue color. During the course of this conversion to deliver **1**, the following reactions were considered to occur:



Reactions 1-5 describe varying degrees of charge transfer from lithium peroxide to benzoquinone. Reaction **1**, which depicts the formation of an adsorption layer of benzoquinone on lithium peroxide, may be ruled out on the basis of the

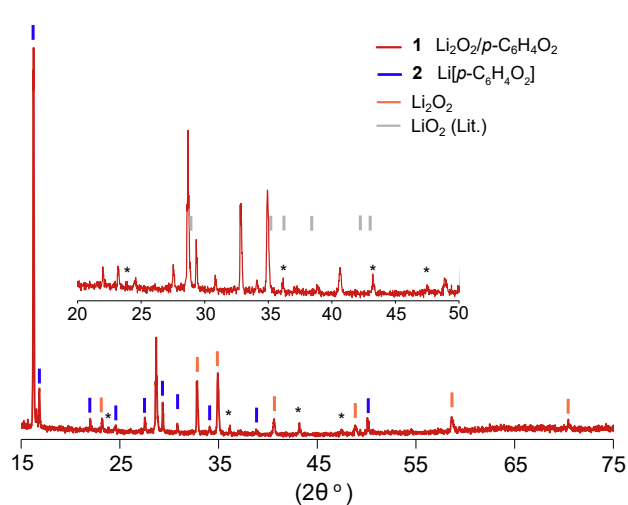


**Fig. 9.** PXRD pattern of **1** (red). Lithium peroxide and **2** are observed in **1** and are indicated with orange and blue marks, respectively. Several unknown diffraction peaks are marked with asterisks. The inset shows a select region of the PXRD pattern along with gray marks indicating the position of peaks that have been previously ascribed to  $\text{LiO}_2$  (34). The PXRD was recorded with Ni-filtered  $\text{Cu-K}\alpha$  radiation.

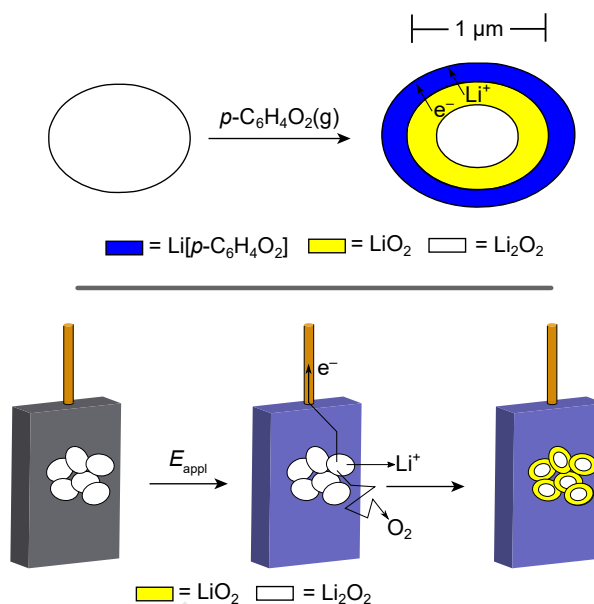


**Fig. 10.** Schematic representation of **1** (top) assuming the material starts from a  $1\ \mu\text{m}$  sphere of  $\text{Li}_2\text{O}_2$ . The analogy of **1** to a charging electrode is represented in the bottom panel.

of  $\text{Li}[p\text{-C}_6\text{H}_4\text{O}_2]$  as a component of **1**. The PXRD pattern of **1** shown in Fig. 9 has peaks coincident with those of **2** prepared by mechanical comproportionation of  $\text{Li}_2[p\text{-C}_6\text{H}_4\text{O}_2]$  and  $p\text{-C}_6\text{H}_4\text{O}_2$ . Remaining peaks present in the pattern of **1** are assigned either to  $\text{Li}_2\text{O}_2$  or unknown phase(s). Several computational studies have predicted that the lowest energy structure of  $\text{LiO}_2$  is the orthorhombic phase (64–66). Although possible correspondence of the observed pattern with that of a simulated pattern derived from *ab initio* calculations (64–66) occurs near  $2\theta = 35^\circ$ , and the peaks labeled with asterisks in Fig. 9 are coincident with peaks assigned as  $\text{LiO}_2$  (34), definitive assignment of the unknown peaks cannot be made nor can it be determined whether  $\text{LiO}_2$ , if present in **1**, is amorphous.

O K-edge XAS of **1**, **2**,  $\text{Li}_2[p\text{-C}_6\text{H}_4\text{O}_2]$ , and  $\text{Li}_2\text{O}_2$  demonstrate marked differences between the samples. Differentiating features are observed in the spectra of **2** and  $\text{Li}_2[p\text{-C}_6\text{H}_4\text{O}_2]$ , providing additional evidence for disproportionation of  $\text{Li}_2[p\text{-C}_6\text{H}_4\text{O}_2]$  and  $p\text{-C}_6\text{H}_4\text{O}_2$ . The presence of **2** and  $\text{Li}_2\text{O}_2$  as a component of **1** obscures the pre-edge region of the O K-edge XAS spectrum of **1** where  $\text{LiO}_2$  has been previously measured in matrices (67), precluding its definitive identification.

The formulation of **1** may be addressed having established that **1** is composed of  $\text{Li}[p\text{-C}_6\text{H}_4\text{O}_2]$  and  $\text{Li}_2\text{O}_2$  and inferred the presence of  $\text{LiO}_2$  through EPR, PXRD, and titration methods. Elemental analysis of **1** consistently indicates a formula of  $[\text{Li}_2\text{O}_2] \cdot [p\text{-C}_6\text{H}_4\text{O}_2]_{0.7}$  yet spectroscopic analysis indicates that the redox level of  $p\text{-C}_6\text{H}_4\text{O}_2$  is that of a monoanion. To accommodate the redox level of  $p\text{-benzoquinone}$ , a commensurate number of lithium ions and electrons must be drawn from  $\text{Li}_2\text{O}_2$ . In the context of reaction 2, a more detailed formula of **1** including speciation is proposed to be  $[\text{Li}_2\text{O}_2]_{0.3} \cdot [\text{LiO}_2]_{0.7} \cdot \{\text{Li}[p\text{-C}_6\text{H}_4\text{O}_2]\}_{0.7}$ . Why  $\text{Li}_2\text{O}_2$  stops absorbing  $p\text{-C}_6\text{H}_4\text{O}_2$  after 0.7 equivalents is currently unknown but may be related to particle size.

A schematic representation of **1** is provided in Fig. 10.

absorptions assigned as  $\text{Li}[p\text{-C}_6\text{H}_4\text{O}_2]$  dominate the UV-vis spectrum of **1**, however, small deviations of the spectrum of **1** relative to **2** indicate an additional band at 265 nm that may be that of superoxide.

Other spectroscopic data (resonance Raman, IR and EPR) point to the presence of **2** as a component of **1**. The Raman spectrum of **1** is overlaid with that of **2** in Fig. 7. The agreement between the spectra confirms that  $\text{Li}[p\text{-C}_6\text{H}_4\text{O}_2]$  is present in both samples and has not been chemically altered in **1**. Additionally, Raman spectra taken at time points corresponding to low coverages of **2** on **1** indicate the presence of a species consistent with a superoxide O–O stretch at  $1139\ \text{cm}^{-1}$ . The EPR spectra of **1** and **2** are dominated by a broad featureless absorption at  $g = 2.008$ ; however, the spectrum of **1** displays a significantly narrower signal. The superposition of a broad and narrow absorption has been noted for samples of potassium superoxide, with the broad line ascribed to the majority of the strong exchange-coupled superoxide anions present in the sample and the narrow line attributed to a very small population (approximately 1 in every  $10^4$  spins) of superoxide anions that are able to freely rotate in the sample and have poor electronic coupling with their environment (45). The EPR spectrum of **1** is dominated by features arising from  $\text{Li}[p\text{-C}_6\text{H}_4\text{O}_2]$ , but the absence of the narrow absorption in the spectrum of **2** suggests that this feature is unique to **1** and may be tentatively assigned as arising from the superoxide ion. The presence of this feature is not observed uniformly across all preparations of **1**, presumably due to the extremely small percentage of spins contributing to this narrow line. The EPR spectrum of  $\text{Li}[p\text{-C}_6\text{H}_4\text{O}_2]$  has been observed in prior work, (57, 60) with the notable observation of hyperfine structure when EPR spectra were recorded with dilute samples. Loss of hyperfine structure in spectra of  $\text{Li}[p\text{-C}_6\text{H}_4\text{O}_2]$  is seen for concentrated samples (60). The latter observation is consonant with the lack of hyperfine structure seen for solid samples of **1** and **2**.

PXRD analysis lends further support to the assignment

Commercial lithium peroxide is composed of particles with a diameter on the order of several hundred nanometers (Fig. 2). Raman and IR spectroscopy clearly indicate the presence of **2** on the surface of **1**. The Li[*p*-C<sub>6</sub>H<sub>4</sub>O<sub>2</sub>] forms a shell about Li<sub>2</sub>O<sub>2</sub> with a thickness of approximately one quarter of the diameter of the Li<sub>2</sub>O<sub>2</sub> particle based upon a density of ca. 1.6 g/cm<sup>3</sup> for **2**. Notably, the schematic shown in Fig. 10 resembles that of theoretical models(68) and experimental studies(69, 70) which propose an amorphous LiO<sub>2</sub> shell around a crystalline Li<sub>2</sub>O<sub>2</sub> core in non-aqueous Li-O<sub>2</sub> batteries. The lithium peroxide core is believed to be the source of both lithium ions and electrons resulting in the formation of LiO<sub>2</sub>. The shell of Li[*p*-C<sub>6</sub>H<sub>4</sub>O<sub>2</sub>] may be crucial for kinetic stabilization of the thermodynamically unstable LiO<sub>2</sub> layer against disproportionation to Li<sub>2</sub>O<sub>2</sub> and O<sub>2</sub>. A recent computational and experimental study concluded that interfacial charge transfer from LiO<sub>2</sub> to the electrolyte may be responsible for the observed stability of LiO<sub>2</sub> (66). A degree of charge transfer from LiO<sub>2</sub> to Li[*p*-C<sub>6</sub>H<sub>4</sub>O<sub>2</sub>] in **1** is expected based upon the reduction potentials of the relevant species presented in Figure 3, providing a plausible explanation for the resistance of LiO<sub>2</sub> to disproportionation in **1** in addition to physical confinement.

At the center of the particle in Fig. 10, crystalline Li<sub>2</sub>O<sub>2</sub> remains and accounts for the substoichiometric ratio of *p*-C<sub>6</sub>H<sub>4</sub>O<sub>2</sub> relative to Li<sub>2</sub>O<sub>2</sub>. Upon heating above 70 °C, the coating layer of Li[*p*-C<sub>6</sub>H<sub>4</sub>O<sub>2</sub>] disproportionates into Li<sub>2</sub>[*p*-C<sub>6</sub>H<sub>4</sub>O<sub>2</sub>] and *p*-C<sub>6</sub>H<sub>4</sub>O<sub>2</sub>. An earlier study noted that adding an alkali base to a mixture of *p*-C<sub>6</sub>H<sub>4</sub>O<sub>2</sub> and hydroquinone (*p*-C<sub>6</sub>H<sub>4</sub>(OH)<sub>2</sub>) resulted in the alkali base developing a blue color, which was believed to be due to trapped benzoquinone radical anions on the surface of the alkali base support (71). This result is particularly interesting because it suggests a strategy to prepare unstable intermediates with adsorption on a reactive support surface, which has been utilized in this present study. In the core-shell structure of **1** there are two components determining electron and ion conduction throughout the material: the LiO<sub>2</sub> core and a Li[*p*-C<sub>6</sub>H<sub>4</sub>O<sub>2</sub>] shell. With regard to the core, recent experimental(72) and first-principles studies(73–75) have indicated that LiO<sub>2</sub> possesses remarkable ionic and electronic conductivities, greatly exceeding that of other alkali superoxides and peroxides(75), presumably crucial properties necessary to form the structure shown in Fig. 10. The other component of the structure in Fig. 10 is Li[*p*-C<sub>6</sub>H<sub>4</sub>O<sub>2</sub>]. Micron-thick films of Li[*p*-C<sub>6</sub>H<sub>4</sub>O<sub>2</sub>] have been previously prepared *via* electrodeposition of *p*-C<sub>6</sub>H<sub>4</sub>O<sub>2</sub> from a lithium-ion containing electrolyte(43). Deposition of thick films of Li[*p*-C<sub>6</sub>H<sub>4</sub>O<sub>2</sub>] highlight the excellent conductivity of this material, however, the counterbalancing lithium cation need only be deposited on the surface of the growing film from solution. In contrast, in forming the core-shell structure of **1**, lithium cations must diffuse from the core to the outer surface of the shell. Thus, termination of **1** with a core-shell structure suggests that the lithium-ion mobility of the shell is kinetically limiting. The schematic presented in Figure 10 along with qualitative observations of the electrical and ionic conductivity of the constituents of **1** may also explain why **1** does not absorb more than 0.7 equivalents of *p*-C<sub>6</sub>H<sub>4</sub>O<sub>2</sub>. At the early stages of the reaction in which **1** is formed from Li<sub>2</sub>O<sub>2</sub> and *p*-C<sub>6</sub>H<sub>4</sub>O<sub>2</sub>, the area of the interface between LiO<sub>2</sub> and Li<sub>2</sub>O<sub>2</sub> is large allowing for lithium and electron transfer

from Li<sub>2</sub>O<sub>2</sub> despite its poor conductivity. However, as the reaction progresses, this interface drastically shrinks in size and ultimately the rate of the reaction becomes limited by the poor conductivity of Li<sub>2</sub>O<sub>2</sub>. Additionally, disproportionation of LiO<sub>2</sub> at the Li[*p*-C<sub>6</sub>H<sub>4</sub>O<sub>2</sub>]/Li<sub>2</sub>O<sub>2</sub> interface may place a poorly conducting barrier between the quinone and original particle.

Several recent publications have used benzoquinone and anthraquinone derivatives as soluble redox mediators in lithium-air batteries (76). 2,5-di-*tert*-butyl-1,4-benzoquinone was found to enhance the rate of ORR and drastically increase the capacity of a lithium-air cells (77, 78). Another study found that benzoquinone exhibited the best performance as a redox mediator based on cathodic chronopotentiometry, although detection of lithium peroxide via XPS was the sole physical characterization method (79), while another study has suggested an explicit interaction between anthraquinone and LiO<sub>2</sub> in solution (80). Importantly, in the present study, the solvent-free conditions employed enforce physical confinement of the lithium peroxide/superoxide layer which may be crucial in stabilizing thermodynamically unstable lithium superoxide. This strategy of physical confinement may also be crucial in ameliorating lithium superoxide induced solvent degradation, a key challenge to overcome if higher cycling numbers are to be achieved in lithium-air batteries (15, 29, 81–83).

## Conclusions

Exposure of solid Li<sub>2</sub>O<sub>2</sub> to *p*-C<sub>6</sub>H<sub>4</sub>O<sub>2</sub> results in the formation of a dark black material. This material has been investigated by a variety of spectroscopic methods and is best described as a coating of Li[*p*-C<sub>6</sub>H<sub>4</sub>O<sub>2</sub>] on LiO<sub>2</sub> and Li<sub>2</sub>O<sub>2</sub>. This reaction is unique in that electron transfer from Li<sub>2</sub>O<sub>2</sub> occurs with *p*-C<sub>6</sub>H<sub>4</sub>O<sub>2</sub> resulting in a comproportionation-like reaction. This reaction methodology can be extended to the preparation of the quinone radical anion from Li<sub>2</sub>[*p*-C<sub>6</sub>H<sub>4</sub>O<sub>2</sub>] and *p*-C<sub>6</sub>H<sub>4</sub>O<sub>2</sub>. The preparation of **1** and compounds similar to **1** allow for controlled “snapshots” of lithium peroxide during the electron transfer from Li<sub>2</sub>O<sub>2</sub> to electron acceptors (redox shuttles). Indeed, we show here that LiO<sub>2</sub> may be stabilized on Li<sub>2</sub>O<sub>2</sub> surfaces in the presence of the electron accepting *p*-C<sub>6</sub>H<sub>4</sub>O<sub>2</sub>, which as highlighted in Fig. 10 is a surrogate for the anode of a lithium-air battery. By careful control of the potential of the electron acceptor and concentration, it may be possible to intimately study the properties of electron deficient Li<sub>2</sub>O<sub>2</sub>, LiO<sub>2</sub> and the ‘superoxide like’ sites, which crucially contribute to the conductivity of Li<sub>2</sub>O<sub>2</sub>. Furthermore, a strategy of molecular encapsulation of Li<sub>2</sub>O<sub>2</sub> with a conductive layer may serve as a promising method to protect cell components, including the electrolyte, from deleterious degradation reactions initiated by LiO<sub>2</sub> and by extension improve the performance of metal-air batteries.

**Supporting Information (SI).** Full details of experimental procedures for the synthesis of new substances together with characterization data are provided in the SI file.

**ACKNOWLEDGMENTS.** This research was supported by the National Science Foundation CHE-1454455 (K.M.L.) and Department of Energy, Office of Science, Office of Basic Energy Sciences DE-SC0017619 (D.G.N.). Grants from the NSF also provided instrument support to the DCIF at MIT (Grants CHE-9808061 and DBI-9729592). This work was supported in part by Robert Bosch

- 541 LLC through its MITEI Sustaining Membership Agreement. Raman spectra were acquired through the support of the Harvard  
542 Center of Nanoscales Systems and NSF's National Nanotechnology  
543 Infrastructure Network (NNIN). We thank Dr. Sarah S. Park and  
544 Dr. Adam J. Rieth for assistance with physical measurements and  
545 Dr. Miguel Gonzalez and Kay Xia for helpful comments. We additionally thank Prof. Yang Shao-Horn for her helpful advice on  
546 minimizing the fluorescence background of Raman spectra. XAS data were obtained at SSRL, which is supported by the U.S. Department  
547 of Energy, Office of Science, Office of Basic Energy Sciences under Contract No. DE-AC02-76SF00515. The SSRL Structural  
548 Molecular Biology Program is supported by the Department of Energy's Office of Biological and Environmental Research, and by  
549 NIH/HIGMS (including P41GM103393).
- 555 1. K. M. Abraham and Z. Jiang. A polymer electrolyte-based rechargeable lithium/oxygen battery. *J. Electrochem. Soc.*, 143(1):1–5, 1996.
  - 557 2. G. Girishkumar, B. McCloskey, A. C. Luntz, S. Swanson, and W. Wilcke. Lithium-air battery: Promise and challenges. *J. Phys. Chem. Lett.*, 1:2193–2203, 2010.
  - 559 3. Jake Christensen, Paul Albertus, Roel S. Sanchez-Carrera, Timm Lohmann, Boris Kozinsky, Ralf Liedtke, Jasim Ahmed, and Aleksandar Kojic. A critical review of Li/air batteries. *J. Electrochem. Soc.*, 159(2):R1–R30, 2011.
  - 562 4. Yi-Chun Lu, Betar M. Gallant, David G. Kwabi, Jonathon R. Harding, Robert R. Mitchell, M. Stanley Whittingham, and Yang Shao-Horn. Lithium-oxygen batteries: Bridging mechanistic understanding and battery performance. *Energy Environ. Sci.*, 6:750–768, 2013.
  - 565 5. D. Aurbach, B. D. McCloskey, L. F. Nazar, and Peter G. Bruce. Advances in understanding mechanisms underpinning lithium-air batteries. *Nat. Energy*, 1:16128, 2016.
  - 567 6. Xiahui Yao, Qi Dong, Qingmei Cheng, and Dunwei Wang. Why do lithium-oxygen batteries fail: Parasitic chemical reactions and their synergistic effect. *Angew. Chem. Int. Ed.*, 55(38):11344–11353, 2016.
  - 570 7. D.G. Kwabi, N. Ortiz-Vitoriano, S.A. Freunberger, Y. Chen, N. Imanishi, P.G. Bruce, and Y. Shao-Horn. Materials challenges in rechargeable lithium-air batteries. *MRS Bull.*, 39(5):443–452, 005 2014.
  - 573 8. Nika Mahne, Olivier Fontaine, Musthafa Ottakam Thotiyil, Martin Wilkening, and Stefan A. Freunberger. Mechanism and performance of lithium-oxygen batteries - A perspective. *Chem. Sci.*, 8:6716–6729, 2017.
  - 576 9. David G. Kwabi, Michal Tulodziecki, Nir Pour, Daniil M. Itkis, Carl V. Thompson, and Yang Shao-Horn. Controlling solution-mediated reaction mechanisms of oxygen reduction using potential and solvent for aprotic lithium-oxygen batteries. *J. Phys. Chem. Lett.*, 7:1204–1212, 2016.
  - 580 10. Colin M. Burke, Vikram Pande, Abhishek Khetan, Venkatasubramanian Viswanathan, and Bryan D. McCloskey. Enhancing electrochemical intermediate solvation through electrolyte anion selection to increase nonaqueous Li-O<sub>2</sub> battery capacity. *Proc. Natl. Acad. Sci. U. S. A.*, 112(30):9293–9298, 2015.
  - 584 11. Daniel Sharon, Daniel Hirsberg, Michal Afri, Frederick Chesneau, Ronit Lavi, Aryeh A. Frimer, Yang Sun, and Doron Aurbach. Catalytic behavior of lithium nitrate in Li-O<sub>2</sub> cells. *ACS Appl. Mater. Inter.*, 7:1659–1660, 2015.
  - 587 12. K. Uta Schwenke, Michael Metzger, Tassilo Restle, Michele Piana, and Hubert A. Gasteiger. The influence of water and protons on Li<sub>2</sub>O<sub>2</sub> crystal growth in aprotic Li-O<sub>2</sub> cells. *J. Electrochem. Soc.*, 162(4):A573–A584, 2015.
  - 590 13. Nagaphani B. Aetukuri, Bryan D. McCloskey, Jeannette M. Garcia, Leslie E. Krupp, Venkatasubramanian Viswanathan, and Alan C. Luntz. Solvating additives drive solution-mediated electrochemistry and enhance toroid growth in non-aqueous Li-O<sub>2</sub> batteries. *Nat. Chem.*, 7:50–56, 2015.
  - 594 14. David G. Kwabi, Thomas P. Batcho, Chibueze V. Amanchukwu, Nagore Ortiz-Vitoriano, Paula Hammond, Carl V. Thompson, and Yang Shao-Horn. Chemical instability of dimethyl sulfoxide in lithium-air batteries. *J. Phys. Chem. Lett.*, 5:2850–2856, 2014.
  - 597 15. Stefan A. Freunberger, Yuhui Chen, Zhanquan Peng, John M. Griffin, Laurence J. Hardwick, Fanny Bardé, Petr Novák, and Peter G. Bruce. Reactions in the rechargeable lithium-O<sub>2</sub> battery with alkyl carbonate electrolytes. *J. Am. Chem. Soc.*, 133(20):8040–8047, 2011.
  - 600 16. Yuhui Chen, Stefan A. Freunberger, Zhanquan Peng, Fanny Bardé, and Peter G. Bruce. Li-O<sub>2</sub> battery with a dimethylformamide electrolyte. *J. Am. Chem. Soc.*, 134:7952–7957, 2012.
  - 602 17. Abhishek Khetan, Heinz Pitsch, and Venkatasubramanian Viswanatha. Solvent degradation in nonaqueous Li-O<sub>2</sub> batteries: Oxidative stability versus H-abstraction. *J. Phys. Chem. Lett.*, 5:2419–2424, 2014.
  - 605 18. Jeannette M. Garcia, Hans W. Horn, and Julia E. Rice. Dominant decomposition pathways for etheral solvents in Li-O<sub>2</sub> batteries. *J. Phys. Chem. Lett.*, 6:1795–1799, 2015.
  - 607 19. Eléonore Mourad, Yann K. Petit, Riccardo Spezia, Aleksej Samojlov, Francesco F. Summa, Christian Prehal, Christian Leypold, Nika Mahne, Christian Slugovc, Olivier Fontaine, Sergio Brutti, and Stefan A. Freunberger. Singlet oxygen from cation driven superoxide disproportionation and consequences for aprotic metal-O<sub>2</sub> batteries. *Energy Environ. Sci.*, 12:2559–2568, 2019.
  - 612 20. Yu Wang, Ying-Rui Lu, Chung-Li Dong, and Yi-Chun Lu. Critical factors controlling superoxide reactions in lithium-oxygen batteries. *ACS Energy Lett.*, 5(5):1355–1363, 2020.
  - 614 21. Maxwell D. Radin and Donald J. Siegel. Charge transport in lithium peroxide: Relevance for rechargeable metal-air batteries. *Energy Environ. Sci.*, 6:2370–2379, 2013.
  - 616 22. Kah Chun Lau, Jun Lu, Xiangyi Luo, Larry A. Curtiss, and Khalil Amine. Implications of the unpaired spins in Li-O<sub>2</sub> battery chemistry and electrochemistry: A minireview. *ChemPlusChem*, 8(2):336–343, 2015.
  - 618 23. Lester Andrews. Matrix infrared spectrum and bonding in the lithium superoxide molecule, LiO<sub>2</sub>. *J. Am. Chem. Soc.*, 90(26):7368–7370, 1968.
  - 620 24. Lester Andrews. Infrared spectrum, structure, vibrational potential function, and bonding in the lithium superoxide molecule LiO<sub>2</sub>. *J. Chem. Phys.*, 50(10):4288–4299, 1969.
  - 622 25. Lester Andrews. Ultraviolet absorption studies of the alkali metal atom-oxygen molecule matrix reaction. *J. Mol. Spectrosc.*, 61(3):337–345, 1976.
  - 624 26. D. M. Lindsay and D. A. Garland. ESR spectra of matrix-isolated lithium superoxide. *J. Phys. Chem.*, 91(24):6158–6161, 1987.
  - 626 27. Xuefeng Wang and Lester Andrews. Infrared spectra, structure and bonding in the LiO<sub>2</sub>, LiO<sub>2</sub>Li, LiO and Li<sub>2</sub>O molecules in solid neon. *Mol. Phys.*, 107:739–748, 2009.
  - 628 28. I. I. Vol'nov, S. A. Tokareva, V. N. Belevskii, and V. I. Klimanov. Investigation of the nature of the interaction of lithium peroxide with ozone. *Russ. Chem. Bull.*, 16:1369–1371, 1967.
  - 629 29. Xinmin Zhang, Limin Guo, Linfeng Gan, Yantao Zhang, Jing Wang, Lee R. Johnson, Peter G. Bruce, and Zhanquan Peng. LiO<sub>2</sub>: Cryosynthesis and chemical/electrochemical reactivities. *J. Phys. Chem. Lett.*, 8(10):2334–2338, 2017.
  - 631 30. Jun Lu, Yun Jung Lee, Xiangyi Luo, Kah Chun Lau, Mohammad Asadi, Scott Brombosz Hsien-Hau Wang, Jianguo Wen, Dengyun Zhai, Zonghai Chen, Dean J. Miller, Yo Sub Jeong, Jin-Bum Park, Zhigang Zak Fang, Bijandra Kumar, Amin Salehi-Khojin, Yang-Kook Sun, Larry A. Curtiss, and Khalil Amine. A lithium-oxygen battery based on lithium superoxide. *Nature*, 529:377–382, 2016.
  - 633 31. Junbing Yang, Dengyun Zhai, Hsien-Hau Wang, Kah Chun Lau, John A. Schlueter, Peng Du, Deborah J. Myers, Yang-Kook Sun, Larry A. Curtiss, and Khalil Amine. Evidence for lithium superoxide-like species in the discharge product of a Li-O<sub>2</sub> battery. *Phys. Chem. Chem. Phys.*, 15:3764–3771, 2013.
  - 635 32. Forrest S. Gittleton, Koffi P. C. Yao, David G. Kwabi, Sayed Youssef Sayed, Won-Hee Ryu, Yang Shao-Horn, and André D. Taylor. Raman spectroscopy in lithium-oxygen battery systems. *ChemElectroChem*, 2(10):1446–1457, 2015.
  - 637 33. Joseph K. Papp, Jason D. Forster, Colin M. Burke, Hyo Won Kim, Alan C. Luntz, Robert M. Shelby, Jeffrey J. Urban, and Bryan D. McCloskey. Poly(vinylidene fluoride) (PVDF) binder degradation in Li<sub>2</sub>O<sub>2</sub> batteries: A consideration for the characterization of lithium superoxide. *J. Phys. Chem. Lett.*, 8(6):1169–1174, 2017.
  - 639 34. Avik Halder, Hsien-Hau Wang, Kah Chun Lau, Rajeev S. Assary, Jun Lu, Stefan Vajda, Khalil Amine, and Larry A. Curtiss. Identification and implications of lithium superoxide in Li-O<sub>2</sub> batteries. *ACS Energy Lett.*, 3(5):1105–1109, 2018.
  - 641 35. Won-Jin Kwak, Jin-Bum Park, Hun-Gi Jung, and Yang-Kook Sun. Controversial topics on lithium superoxide in Li-O<sub>2</sub> batteries. *ACS Energy Lett.*, 2(12):2756–2760, 2017.
  - 643 36. C. G. de Kruij, E. J. Smit, and H. A. J. Govers. Thermodynamic properties of 1,4-benzoquinone (BQ), 1,4-hydroquinone (HQ), 1,4-naphthoquinone (NQ), 1,4-naphthohydroquinone (NHQ), and the complexes BQ-HQ 1:1, NQ-HQ 1:1, NQ-NHQ 2:1, and NQ-NHQ 1:1. *J. Chem. Phys.*, 74(10):5838–5841, 1981.
  - 645 37. Henry G. Kuivila. Electrophilic displacement reactions. III. Kinetics of the reaction between hydrogen peroxide and benzenboronic acid. *J. Am. Chem. Soc.*, 76(3):870–874, 1954.
  - 647 38. Jian-Ming Lü, Sergiy V. Rosokha, and Jay K. Kochi. Stable (long-bonded) dimers via the quantitative self-association of different cationic, anionic, and uncharged  $\pi$ -radicals: Structures, energetics, and optical transitions. *J. Am. Chem. Soc.*, 125:12161–12171, 2003.
  - 649 39. Sergiy V. Rosokha, Jianjiang Lu, Tetyana Y. Rosokha, and Jay K. Kochi. Counter-ion modulation of long-distance  $\pi$ -bonding of the open-shell p-benzoquinone anions. *Phys. Chem. Chem. Phys.*, 11:324–332, 2009.
  - 651 40. Zhiping Song, Yumin Qian, Tao Zhang, Minoru Otani, and Haoshen Zhou. Poly(benzoquinonyl sulfide) as a high-energy organic cathode for rechargeable Li and Na batteries. *Adv. Sci.*, 2(9):1500124, 2015.
  - 653 41. Lee Johnson, Chunmei Li, Zheng Liu, Yuhui Chen, Stefan A. Freunberger, Praveen C. Ashok, Bavishna B. Praveen, Kishan Dholakia, Jean-Marie Tarascon, and Peter G. Bruce. The role of Li<sub>2</sub>O solubility in O<sub>2</sub> reduction in aprotic solvents and its consequences for Li-O<sub>2</sub> batteries. *Nature Chem.*, 6:1091–1099, 2014.
  - 655 42. Harald Gamp and Stephen J. Lippard. Reinvestigation of 18-crown-6 ether/potassium superoxide solutions in Me<sub>2</sub>SO. *Inorg. Chem.*, 22:357–358, 1983.
  - 657 43. A. Desbène-Monvernay, P.C. Lacaze, and A. Cherigui. UV-visible spectroelectrochemical study of some para- and ortho-benzoquinoid compounds: Comparative evaluation of their electrochromic properties. *J. Electroanal. Chem. Interfac.*, 260(1):75–90, 1989.
  - 659 44. Yoshio Matsunaga. The electron spin resonance absorption spectra of some semiquinone ions: Part III. Free radical salts of quinhydrone. *Can. J. Chem.*, 38(7):1172–1176, 1960.
  - 661 45. Ahsan U. Khan and S. D. Mahanti. Collective electron effects of O<sub>2</sub><sup>-</sup> in potassium superoxide. *J. Chem. Phys.*, 63(6):2271–2278, 1975.
  - 663 46. Jenee D. Cyran, Jacob M. Nite, and Amber T. Krummel. Characterizing anharmonic vibrational modes of quinones with two-dimensional infrared spectroscopy. *J. Phys. Chem. B*, 119:8917–8925, 2015.
  - 665 47. Xiaojie Zhao, Hiroshi Imahori, Chang-Guo Zhan, Yoshiteru Sakata, Suehiro Iwata, and Teizo Kitagawa. Resonance Raman and FTIR spectra of isotope-labeled reduced 1,4-benzoquinone and its protonated forms in solutions. *J. Phys. Chem.*, 101:622, 1997.
  - 667 48. Satish C. B. Myneni. Soft X-ray spectroscopy and spectromicroscopy studies of organic molecules in the environment. *Rev. Mineral Geochem.*, 49(1):485–579, 2002.
  - 669 49. J. T. Francis and A. P. Hitchcock. Inner-shell spectroscopy of p-benzoquinone, hydroquinone, and phenol: Distinguishing quinoid and benzenoid structures. *J. Phys. Chem.*, 96:6598–6610, 1992.
  - 671 50. U. Couhorn and R. Dronskowski. Alkali metal compounds of hydroquinone: Synthesis and crystal structure. *Z. Anorg. Allg. Chem.*, 629:647–652, 2003.
  - 673 51. Alexander R. Lippert, Genevieve C. Van de Bittner, and Christopher J. Chang. Boronate oxidation as a bioorthogonal reaction approach for studying the chemistry of hydrogen peroxide in living systems. *Acc. Chem. Res.*, 44(9):793–804, 2011.
  - 675 52. Balaraman Kalyanaraman, Micael Hardy, Radoslaw Podsiadly, Gang Cheng, and Jacek Zielonka. Recent developments in detection of superoxide radical anion and hydrogen peroxide: Opportunities, challenges, and implications in redox signaling. *Arch. Biochem. Biophys.*, 617:38–47, 2017.
  - 677 53. Yong Che, Manabu Tsushima, Futoshi Matsumoto, Takeyoshi Okajima, Koichi Tokuda, and Takeo Ohsaka. Water-induced disproportionation of superoxide ion in aprotic solvents. *J. Phys. Chem.*, 100(51):20134–20137, 1996.
  - 679 54. Krzysztof Piech, Thomas Bally, Takatoshi Ichino, and John Stanton. Vibronic spectra of the

- p-benzoquinone radical anion and cation: A matrix isolation and computational study. *Phys. Chem. Chem. Phys.*, 16:2011–2019, 2014.
55. Andrew R. Cook, Larry A. Curtiss, and John R. Miller. Fluorescence of the 1,4-benzoquinone radical anion. *J. Am. Chem. Soc.*, 119(24):5729–5734, 1997.
56. Jian-Ming Lü, Sergiy V. Rosokha, Ivan S. Neretin, and Jay K. Kochi. Quinones as electron acceptors. X-ray structures, spectral (EPR, UV-vis) characteristics and electron-transfer reactivities of their reduced anion radicals as separated vs contact ion pairs. *J. Am. Chem. Soc.*, 128:16708–16719, 2006.
57. E. A. C. Lucken. 814. Ion-association and specific solvation in the electron spin resonance spectra of semiquinones. *J. Chem. Soc.*, pages 4234–4240, 1964.
58. Masaaki Yashiro and Kazuo Sato. A new electrochromic material: 1,4-Benzoquinone in a non-aqueous solution. *Jpn. J. Appl. Phys.*, 20(7):1319, 1981.
59. K.J. Stutts and G.W. Eastland. The lithium salt of benzoquinone radical anion and voltammetric anomalies. *J. Electroanal. Chem. Interf. Electrochem.*, 235(1):357–359, 1987.
60. Martyn A. Brown, Bruce R. McGarvey, and Dennis G. Tuck. Structure of lithium-p-semiquinonates in non-aqueous solutions. *J. Chem. Soc., Dalton Trans.*, pages 1371–1376, 1998.
61. Xiaojie Zhao and Teizo Kitagawa. Solvent effects of 1,4-benzoquinone and its anion radicals probed by resonance Raman and absorption spectra and their correlation with redox potentials. *J. Raman Spectrosc.*, 29(9):773–780, 1998.
62. Gideon Czapski and Leon M. Dorfman. Pulse radiolysis studies. V. Transient spectra and rate constants in oxygenated aqueous solutions. *J. Phys. Chem.*, 68:1169–1177, 1964.
63. I. B. C. Matheson and John Lee. The absorption spectrum of superoxide anion in dimethylsulfoxide. *Spectroscopy Letters*, 2(4):117–119, 1969.
64. Nicola Seriani. *Ab initio* thermodynamics of lithium oxides: From bulk phases to nanoparticles. *Nanotechnology*, 20(44):445703, 2009.
65. Kah Chun Lau, Larry A. Curtiss, and Jeffrey Greeley. Density functional investigation of the thermodynamic stability of lithium oxide bulk crystalline structures as a function of oxygen pressure. *J. Phys. Chem. C*, 115(47):23625–23633, 2011.
66. Dengyun Zhai, Kah Chun Lau, Hsien-Hau Wang, Jianguo Wen, Dean J. Miller, Jun Lu, Feiyu Kang, Baohua Li, Wenge Yang, Jing Gao, Ernesto Indacochea, Larry A. Curtiss, and Khalil Amine. Interfacial effects on lithium superoxide disproportionation in Li-O<sub>2</sub> batteries. *Nano Lett.*, 15(2):1041–1046, 2015.
67. M. W. Ruckman, Jie Chen, S. L. Qiu, P. Kuiper, Myron Strongin, and B. I. Dunlap. Interpreting the near edges of O<sub>2</sub> and O<sub>2</sub><sup>-1</sup> in alkali-metal superoxides. *Phys. Rev. Lett.*, 67:2533–2536, Oct 1991.
68. Michael J. Welland, Kah Chun Lau, Paul C. Redfern, Linyun Liang, Dengyun Zhai, Dieter Wolf, and Larry A. Curtiss. An atomistically informed mesoscale model for growth and coarsening during discharge in lithium-oxygen batteries. *J. Chem. Phys.*, 143(22):224113, 2015.
69. Yi-Chun Lu and Yang Shao-Horn. Probing the reaction kinetics of the charge reactions of nonaqueous Li-O<sub>2</sub> batteries. *J. Phys. Chem. Lett.*, 4(1):93–99, 2013.
70. Dengyun Zhai, Hsien-Hau Wang, Kah Chun Lau, Jing Gao, Paul C. Redfern, Feiyu Kang, Baohua Li, Ernesto Indacochea, Ujjal Das, Ho-Hyun Sun, Ho-Jin Sun, Khalil Amine, and Larry A. Curtiss. Raman evidence for late stage disproportionation in a Li-O<sub>2</sub> battery. *J. Phys. Chem. Lett.*, 5(15):2705–2710, 2014.
71. D. Bijl, H. Kainer, and A.C. Rose-Innes. Stabilization of free radicals by adsorption: Detection by paramagnetic resonance. *Nature*, 174:830–831, 1954.
72. Samuel T. Plunkett, Hsien-Hau Wang, Se Hwan Park, Yun Jung Lee, Jordi Cabana, Khalil Amine, Said Al-Hallaj, Brian P. Chaplin, and Larry A. Curtiss. Charge transport properties of lithium superoxide in Li-O<sub>2</sub> batteries. *ACS Appl. Energy Mater.*, 3(12):12575–12583, 2020.
73. Byungju Lee, Jinsoo Kim, Gabin Yoon, Hee-Dae Lim, In-Suk Choi, and Kisuk Kang. Theoretical evidence for low charging overpotentials of superoxide discharge products in metal-oxygen batteries. *Chem. of Mater.*, 27(24):8406–8413, 2015.
74. Shunning Li, Jianbo Liu, and Baixin Liu. First-principles study of the charge transport mechanisms in lithium superoxide. *Chem. Mater.*, 29(5):2202–2210, 2017.
75. Nicolai Rask Mathiesen, Sheng Yang, Juan Maria García-Lastra, Tejs Vegge, and Donald J. Siegel. Charge transport in alkali-metal superoxides: A systematic first-principles study. *Chem. Mater.*, 31(21):9156–9167, 2019.
76. Yantao Zhang, Liang Wang, Xiaozheng Zhang, Limin Guo, Ying Wang, and Zhangquan Peng. High-capacity and high-rate discharging of a Coenzyme Q10-catalyzed Li-O<sub>2</sub> battery. *Adv. Mat.*, 30(5):1705571, 2018.
77. Xiangwen Gao, Yuhui Chen, Lee Johnson, and Peter G. Bruce. Promoting solution phase discharge in Li-O<sub>2</sub> batteries containing weakly solvating electrolyte solutions. *Nat. Mater.*, 15:882–888, 2016.
78. Zhen-Zhen Shen, Shuang-Yan Lang, Yang Shi, Jian-Min Ma, Rui Wen, and Li-Jun Wan. Revealing the surface effect of the soluble catalyst on oxygen reduction/evolution in Li-O<sub>2</sub> batteries. *J. Am. Chem. Soc.*, 141(17):6900–6905, 2019.
79. Shoichi Matsuda, Kazuhito Hashimoto, and Shuji Nakanishi. Efficient Li<sub>2</sub>O<sub>2</sub> formation via aprotic oxygen reduction reaction mediated by quinone derivatives. *J. Phys. Chem. C*, 118(32):18397–18400, 2014.
80. Peng Zhang, Liangliang Liu, Xiaofeng He, Xiao Liu, Hua Wang, Jinling He, and Yong Zhao. Promoting surface-mediated oxygen reduction reaction of solid catalysts in metal-O<sub>2</sub> batteries by capturing superoxide species. *J. Am. Chem. Soc.*, 141(15):6263–6270, 2019.
81. Stefan A. Freunberger, Yuhui Chen, Nicholas E. Drewett, Laurence J. Hardwick, Fanny Bardé, and Peter G. Bruce. The lithium-oxygen battery with ether-based electrolytes. *Angew. Chem. Int. Ed.*, 50(37):8609–8613, 2011.
82. Moran Balaish, Alexander Kraysberg, and Yair Ein-Eli. A critical review on lithium-air battery electrolytes. *Phys. Chem. Chem. Phys.*, 16:2801–2822, 2014.
83. Tao Liu, J. Padmanabhan Vivek, Evan Wenbo Zhao, Jiang Lei, Nuria Garcia-Araez, and Clare P. Grey. Current challenges and routes forward for nonaqueous lithium-air batteries. *Chem. Rev.*, 120(14):6558–6625, 2020.